

#### Available online at website: https://journal.bcrec.id/index.php/bcrec

Bulletin of Chemical Reaction Engineering & Catalysis, 20 (3) 2025, 441-457



Original Research Article

## Methylene Blue Degradation with Sulfonated SPG20 Silica-Fe<sub>2</sub>O<sub>3</sub> Hybrid Photocatalysts

Maria Ulfa\*, Pramesta Rosa Salsabila, Agung Nugroho Catur Saputro, Nanik Dwi Nurhayati

Chemistry Education Study Program, Faculty of Teacher Training and Education, Sebelas Maret University, Jl. Ir. Sutami 36A, Surakarta 57126, Indonesia.

Received: 18th April 2025; Revised: 28th May 2025; Accepted: 1st June 2025 Available online: 4th June 2025; Published regularly: October 2025



#### Abstract

This study aims to synthesize and evaluate the photocatalytic performance of a modified mesoporous silica-based composite,  $Fe_2O_3/SPG_{20}$ — $SO_3H$ , for methylene blue degradation. The catalyst was prepared via a soft-template method using P123 surfactant and gelatin as dual structure-directing agents. Characterization results confirmed the formation of  $Fe_2O_3$  crystallites with a dominant size of 2.14 nm and crystallinity of 90.85%. FTIR spectra revealed the presence of –COOH, Si–O–Si, Si–OH, and –OH groups, while sulfonate-related bands (–SO<sub>3</sub>H, O=S=O) were not observed in XRD patterns, suggesting amorphous or poorly crystalline sulfonic groups. SEM analysis indicated rod-like catalyst morphology. Photocatalytic testing under various temperatures showed that  $Fe_2O_3/SPG_{20}$ — $SO_3H$  achieved the highest degradation efficiency at 70 °C, maintaining over 92.14 % efficiency for up to 120 minutes of contact time. Lower temperatures (5 °C and 15 °C) led to reduced and less stable degradation activity. These results indicate that both sulfonation and iron oxide impregnation, combined with optimal operating temperature, significantly enhance the photocatalytic performance of mesoporous silica systems, offering a cost-effective and environmentally friendly solution for dye-contaminated wastewater treatment.

Copyright © 2025 by Authors, Published by BCREC Publishing Group. This is an open access article under the CC BY-SA License (https://creativecommons.org/licenses/by-sa/4.0).

**Keywords**: mesoporous silica; sulfonation; Fe<sub>2</sub>O<sub>3</sub>; photocatalysis; soft-template synthesis

How to Cite: Ulfa, M., Salsabila, P.R., Saputro, A.N.C., Nurharyati, N.D. (2025). Methylene Blue Degradation with Sulfonated SPG20 Silica-Fe<sub>2</sub>O<sub>3</sub> Hybrid Photocatalysts. Bulletin of Chemical Reaction Engineering & Catalysis, 20 (3), 441-457. (doi: 10.9767/bcrec.20380)

Permalink/DOI: https://doi.org/10.9767/bcrec.20380

#### 1. Introduction

The textile industry has shown remarkable growth, fulfilling both domestic and global demands [1]. According to Indonesia's Central Statistics Agency (BPS), the gross domestic product (GDP) at constant prices for the textile industry reached IDR 35.17 trillion in the second quarter of 2022, increasing by 13.74% from the previous year [2]. However, industrial progress also brings environmental challenges—one of the most critical being wastewater contamination from textile dyes [3,4]. Methylene Blue (MB), a widely used synthetic dye, is known for its toxicity

and resistance to degradation [5-7]. With the molecular formula C<sub>16</sub>H<sub>18</sub>ClN<sub>3</sub>S, MB is a cationic aromatic compound that exhibits high solubility and strong coloration. Its persistence in water systems reduces sunlight penetration and oxygen levels, thereby harming aquatic ecosystems [8,9]. Traditional treatment methods such chlorination, ozonation, and biodegradation are often ineffective or economically unfeasible for developing countries [8,9]. Adsorption methods, while common, still leave residual organic cause pollutants that may secondary environmental issues [10,12].

Photocatalysis emerges as a promising alternative for degrading MB in wastewater. This method utilizes semiconductor materials activated by light to produce reactive species, such

\* Corresponding Author. Email: mariaulfa@staff.uns.ac.id (M. Ulfa) as hydroxyl radicals (OH), which break down pollutants [8,13].Metal oxide semiconductors like TiO2, ZnO, and Fe2O3 are widely studied for this application. Among various metal oxides, Fe<sub>2</sub>O<sub>3</sub> is particularly attractive due to its narrow band gap (~2.1 eV), visible-lightdriven activity, low cost, and environmentally benign nature. However, the catalytic efficiency of Fe<sub>2</sub>O<sub>3</sub> alone is often hindered by limited surface area and rapid recombination of photo-generated electron-hole pairs. To overcome these limitations, incorporation of Fe<sub>2</sub>O<sub>3</sub> into mesoporous supports such as silica has been explored to enhance surface area, dispersion, and charge separation, thereby improving photocatalytic performance [13-15]. In this study, mesoporous silica is synthesized using P-123 and gelatin as soft templates. Gelatin, a biodegradable polymer, assists in structuring the pores and enhancing surface functionality [16-18]. The dual-template strategy combines the self-assembly behavior of Pwith the biopolymer-induced network formation of gelatin, potentially leading to hierarchical pore architectures and improved mass transfer characteristics. The silica is further sulfonated to introduce -SO<sub>3</sub>H groups, which improve its adsorption properties and catalytic behavior [17]. Sulfonation introduces Brønsted acid sites that increase the density of adsorption and catalytic sites, while also improving surface polarity. The sulfonation process is temperaturesensitive; thus, various temperatures (room temperature, 70 °C, 90 °C, and 110 °C) are applied to determine optimal conditions [20-22]. To assess this effect more quantitatively, the influence of sulfonation temperature on material color was observed visually and further interpreted based on the corresponding structural changes analyzed in XRD and FTIR data. Although advanced colorimetric or TGA-based quantification was not included, these analyses serve as indirect indicators of sulfonic group incorporation and thermal stability.

Silica-supported iron oxide systems have emerged as effective photocatalysts for the degradation of organic pollutants. Recent studies have shown that mesoporous silica nanospheres with  $Fe_2O_3$ nanoparticles promising photocatalytic activity toward dyes such as methylene blue under visible light irradiation. The silica support plays a crucial role in the uniform distribution of hematite particles, enhancing the catalytic reactivity by preventing agglomeration and increasing the available catalytic sites. Studies have shown that the optimal loading is around 20 wt% Fe<sub>2</sub>O<sub>3</sub>, beyond which agglomeration can reduce the effectiveness [20]. The photocatalytic mechanism mainly involves hydroxyl radicals as the major reactive species, with the composite systems exhibiting good recyclability—an important consideration for

practical applications. However, conventional silica-Fe<sub>2</sub>O<sub>3</sub> systems often face challenges related to limited surface area, poor light absorption, and inefficient charge separation [21].

Although silica-Fe<sub>2</sub>O<sub>3</sub> composites sulfonated materials have been studied separately for methylene blue removal, there is still a significant research gap in systematically integrating sulfonation into photocatalytic systems [17]. Current research how fails to address sulfonation synergistically enhance the adsorption and photocatalytic properties of these materials, which potentially offer dual-functional capabilities that can significantly enhance methylene blue degradation efficiency. Contemporary synthetic approaches typically use a single templating method to create porous structures in silica-based photocatalysts. The present study introduces an innovative dualtemplate route that combines P-123 and gelatin for enhanced mesoporosity, which, to the best of our knowledge, has not yet been systematically applied to sulfonated Fe<sub>2</sub>O<sub>3</sub>-silica systems. Such hierarchical structures can significantly enhance mass transfer, light utilization, and catalytic efficiency.

Fe<sub>2</sub>O<sub>3</sub> nanoparticles are then impregnated into the sulfonated mesoporous silica (SPG20 modified with gelatin) using wet impregnation. Fe<sub>2</sub>O<sub>3</sub> exhibits light absorption within the visible spectrum; however, in this study, a xenon lamp with a UV-visible emission range (200-800 nm) employed, thereby incorporating both ultraviolet and visible light contributions. The synthesized photocatalysts are characterized using X-ray diffraction (XRD), Fourier-transform infrared spectroscopy (FTIR), and UV-Vis diffuse spectroscopy reflectance (DRS). Their photocatalytic activity in degrading Methylene Blue is evaluated via UV-Vis spectrophotometry. This research aims not only to evaluate the photocatalytic performance of the developed material but also to quantitatively investigate the effect of sulfonation temperature on physicochemical properties of Fe<sub>2</sub>O<sub>3</sub>-loaded mesoporous silica. The study contributes to the development of cost-effective and environmentally friendly photocatalysts for dye-contaminated wastewater treatment.

#### 2. Materials and Methods

#### 2.1 Materials

The chemicals used in this study include hydrochloric acid (HCl 37%, Sigma-Aldrich, MW 36.5 g/mol), distilled water (Smart-Lab, MW 18 g/mol), pluronic triblock copolymer P123 (Sigma-Aldrich, MW 5750 g/mol), commercial gelatin (Gelita, MW ~90,000 g/mol), tetraethyl orthosilicate (TEOS, Sigma-Aldrich, MW 208.33

g/mol), methylene blue (Sigma-Aldrich), and iron(III) chloride hexahydrate (FeCl<sub>3</sub> 6H<sub>2</sub>O, Sigma-Aldrich).

## 2.2 Synthesis of Gelatin-Modified Mesoporous Silica (SPG20)

To synthesize SPG20, 4 g of P123 and 0.8 g of gelatin were mixed in 127 mL of diluted HCl solution (19.5 mL of HCl in distilled water), stirred at 40 °C for 3 hours at 500 rpm while HCl was gradually added. Subsequently, 242.08 mL of TEOS was added, and stirring continued for 24 hours. The mixture was then subjected to hydrothermal treatment in an autoclave at 90 °C for 24 hours. The resulting precipitate was filtered, washed, oven-dried at 70 °C and 100 °C sequentially, and then calcined at 550 °C for 5 GSPG20. hours to obtain Structural characterization was conducted using BET (0.05 g), XRD, FTIR, and SEM-EDX (each 0.03 g).

#### 2.3 Activation and Sulfonation of SPG20

For activation, 1.5 g of SPG20 was soaked in 50 mL of 0.1 M HCl for 24 hours, filtered, washed, and dried at 100 °C. The sulfonation process involved reacting 1 g of SPG20 with 10 mL of concentrated  $\rm H_2SO_4$  at varying temperatures (room temp, 70 °C, 90 °C, and 110 °C) under reflux for 20 hours, followed by hot water washing to obtain SPG20–SO<sub>3</sub>H.

## 2.4 Impregnation of Fe<sub>2</sub>O<sub>3</sub> onto SPG20-SO<sub>3</sub>H

A 10%  $Fe_2O_3$  loading was achieved by dissolving 10.102 g  $FeCl_3.6H_2O$  in 30.306 mL distilled water, then mixing with 0.9 g  $SPG_2O_3O_3H$  and stirring at 45 °C for 16 hours. The resulting powder was oven-dried at 160 °C for 2 hours, washed, dried again at 80 °C for 45 minutes, and finally calcined at 450 °C for 4 hours to form  $Fe_2O_3/SPG_2O_3H$ . Characterizations included BET, XRD, FTIR, and SEM-EDX.

## 2.5 Synthesis of Pure Fe<sub>2</sub>O<sub>3</sub> and SiO<sub>2</sub>

For Fe<sub>2</sub>O<sub>3</sub>, FeCl<sub>3</sub>.6H<sub>2</sub>O was dissolved, allowed to settle, centrifuged, filtered, washed, dried at 120 °C for 12 hours, and calcined at 400 °C for 4 hours. For pure SiO<sub>2</sub>, 5 g of TEOS was hydrolyzed in 10 mL water, aged for 24 hours, filtered, dried at 80 °C, and calcined at 550 °C. Structural analysis used XRD, FTIR, BET, and SEM-EDX.

#### 2.6 Photocatalytic Degradation of Methylene Blue

The photocatalytic activity was assessed using 200 mL of 5 ppm MB solution and 50 mg of photocatalyst in a reactor. An adsorption equilibrium was established in the dark for 30 minutes. Then, 10 mL aliquots were transferred

to 12 vials. One vial served as control (t = 0), while others were exposed to UV light and agitation. The UV irradiation was provided by a 25 W xenon lamp ( $\lambda$  = 200–800 nm), which emits a broad spectrum covering both ultraviolet and visible light. The estimated irradiance from a 25 W xenon lamp at a distance of 8 cm is approximately 31.1 mW/cm². Considering the vial's surface area, the photocatalytic sample receives around 55 mW of light power under ideal isotropic emission assumptions. regions. Samples were collected at intervals (0–90 minutes), and MB degradation was monitored by measuring absorbance at 665 nm using UV-Vis spectrophotometry (Shimadzu UV-3600) [22].

#### 2.7 Characterizations

The instruments used for characterizing the samples in this study include X-Ray Diffraction (XRD) from Panalytical (Model PW3050/60), operated within a 20 range of 5° to 80°, to determine the crystallinity and phase composition of the synthesized materials. The surface area and porosity were measured using the Brunauer-Emmett-Teller (BET) method with Quantachrome Nova 1200e instrument. Fourier Transform Infrared Spectroscopy (FTIR), performed using a Shimadzu 21 spectrometer with a resolution of 0.5 cm<sup>-1</sup>, was employed to analyze functional groups in the materials in the wavenumber range of 300-4000 cm<sup>-1</sup>. Scanning Electron Microscopy with Energy Dispersive X-Ray (SEM-EDX) analysis was conducted using a JEOL JSM-700 microscope at a voltage of 15 kV to observe the surface morphology and elemental composition of the samples.

#### 3. Results and Discussion

## 3.1 Synthesis of Gelatin-Modified Mesoporous Silica (SPG20)

The synthesis of gelatin-modified mesoporous silica (SPG20) was accomplished via a softtemplating route employing a binary templating system composed of Pluronic P123 and gelatin. Pluronic P123, a non-ionic triblock copolymer surfactant, was selected due to biocompatibility, low toxicity, and high chemical stability. Gelatin, a natural amphiphilic polymer, was utilized as a co-template to enhance the structural integrity and thermal stability of the mesostructure through synergistic interactions with P123, particularly under acidic conditions [23,27]. The synthesis procedure was initiated by dissolving 4 g of P123 and 1 g of gelatin in 125 mL of 1.6 M HCl at 40 °C under vigorous stirring (500 rpm) for 3 h, yielding a homogeneous, foamy solution. Subsequent addition of tetraethyl orthosilicate (TEOS) as the silica precursor and continuous stirring for 24 h facilitated hydrolysis

polycondensation, yielding a gel-like material. Hydrothermal treatment at 90 °C for 24 h under static conditions in a Teflon-lined autoclave promoted the self-assembly of silica species into an ordered mesostructure. The resulting white gel was subjected to sequential drying at 70 °C and 100 °C, followed by calcination at 550 °C for 5 h to remove residual organics and open the pore structure, producing a fine white powder indicative of successful mesoporous silica formation (Figure 1). This method capitalizes on the dual templating effect to yield a hierarchically porous structure with enhanced hydrothermal stability, wherein gelatin serves as a functional modifier capable of imparting additional surface reactivity for subsequent functionalization steps [25].

## 3.2 Chemical Activation of Gelatin-Modified SPG20

To enhance the surface reactivity and textural properties of SPG20, acid activation was employed using 0.1 M HCl. Approximately 1.5 g of SPG20 was immersed in 50 mL of the acid solution and stirred for 24 h at ambient temperature. This activation step served to remove residual template species and promote the exposure of silanol groups (Si-OH) on the silica framework. Proton exchange and dissolution of surface impurities occurred during this process, which is well-documented to facilitate the formation of Brønsted acid sites conducive to catalytic applications [26]. Posttreatment, the material was thoroughly rinsed with deionized water and oven-dried at 100 °C for 6 h. The resultant white powder exhibited increased brightness and a finer texture, consistent with effective decontamination and activation. This step is essential for improving the accessibility of internal pore spaces and enhancing the material's subsequent reactivity toward sulfonic functionalization (Figure 2).

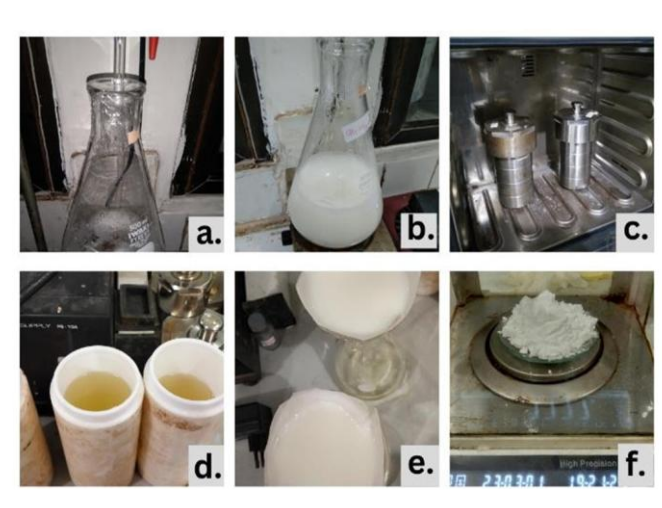


Figure 1. Process of synthesis of gelatin-modified mesoporous silica (SPG20).

#### 3.3 Sulfonation at Variable Temperatures

Sulfonation of the activated SPG20 was conducted to introduce sulfonic acid groups (-SO<sub>3</sub>H) onto the silica surface, which serve as strong Brønsted acid sites and significantly augment the material's catalytic and adsorption capabilities. The sulfonation reactions were performed at four distinct temperatures—5°C, 15 °C, room temperature (~28 °C), and 70 °C—to elucidate the influence of thermal conditions on sulfonic group incorporation. In each experiment, 1 g of activated SPG20 was reacted with 10 mL of concentrated H2SO4 in a three-neck flask fitted with a condenser and thermometer under constant stirring for 12 h. Notably, the reaction at 70 °C yielded a more intense grey-colored slurry, indicative of elevated sulfonation activity and possible partial carbonization of gelatin residues. In contrast, lower temperatures (e.g., 5 °C) yielded paler suspensions, suggesting reduced reactivity (Figure 3).

Following the reaction, each sample was repeatedly washed with hot deionized water (100 °C) until the washings reached neutral pH, to eliminate unreacted H<sub>2</sub>SO<sub>4</sub> and prevent post-sulfonation degradation. During washing,

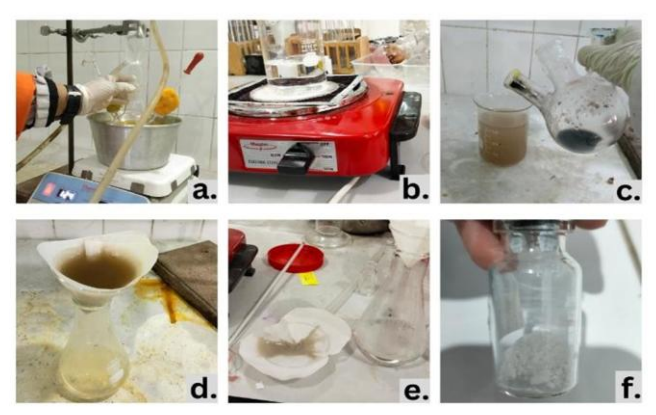


Figure 3. Process of sulfonation.

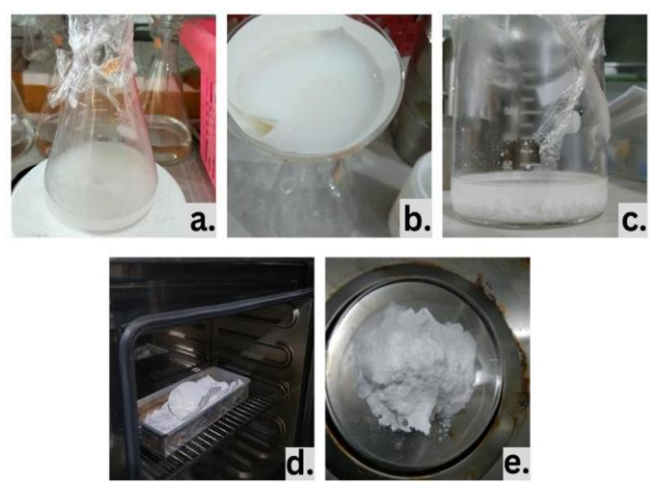


Figure 2. Process of process of chemical activation of gelatin-modified SPG20.

effervescence and vapor release were observed, confirming the exothermic interaction between residual acid and water. The washed solids were then oven-dried at 70 °C for 12 h, producing fine powders ranging from off-white to light grey, depending on the sulfonation temperature. The effectiveness of sulfonation is highly dependent on reaction temperature; elevated temperatures facilitate greater sulfonic group grafting efficiency through improved diffusion kinetics and acid-mediated hydrolysis-condensation mechanisms [27-32]. Thus, the 70 °C treatment is hypothesized to provide the highest density of –SO<sub>3</sub>H functional sites, which is desirable for subsequent catalytic applications.

## $3.4 \text{ Wet Impregnation of Fe}_2\text{O}_3 \text{ onto SPG}20\text{--SO}_3\text{H}$

In order to enhance the photocatalytic performance of the material, iron(III) oxide (Fe<sub>2</sub>O<sub>3</sub>) was impregnated onto the sulfonated SPG20 via the incipient wetness impregnation technique (Figure 4). Fe<sub>2</sub>O<sub>3</sub> serves as a visiblelight active semiconductor with strong redox properties and has been widely employed in the photodegradation of organic pollutants. A loading of 20 wt% Fe<sub>2</sub>O<sub>3</sub> relative to the support mass was employed to ensure adequate photoactivity without excessive pore blockage. The Fe<sub>2</sub>O<sub>3</sub> precursor solution was homogenized with SPG20-SO<sub>3</sub>H, followed by drying and calcination to anchor Fe species within the mesoporous network. This procedure facilitates optimal dispersion of Fe oxide nanoparticles within the matrix, thereby promoting interfacial charge transfer during photocatalytic reactions [29]. The final product exhibited a light reddish-brown hue, consistent with successful iron incorporation and thermal treatment. This composite material, SPG20-SO<sub>3</sub>H/Fe<sub>2</sub>O<sub>3</sub>, is anticipated to exhibit synergistic activity stemming from the acidic functionality of -SO<sub>3</sub>H groups and the photoreactive properties of  $Fe_2O_3$ . Moreover, the gelatin-modified mesoporous silica framework provides a highly accessible and hydrophilic support that enhances

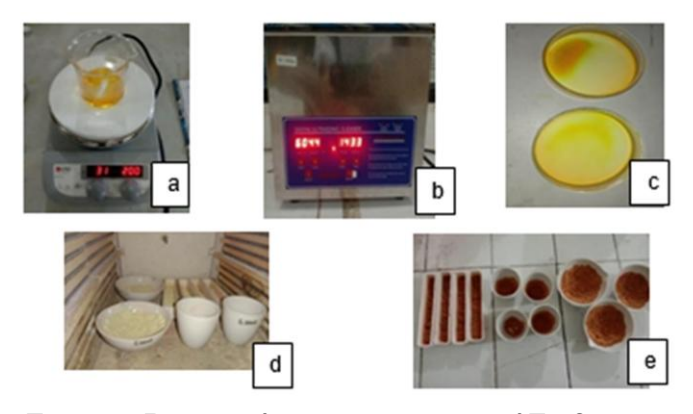


Figure 4. Process of wet impregnation of  $Fe_2O_3$  onto  $SPG20-SO_3H$ .

dye adsorption and facilitates efficient charge separation.

#### 3.5 Overall Evaluation of the Synthesis Protocol

The multistep synthesis protocol—comprising co-templating with gelatin, acid activation, temperature-controlled sulfonation, and Fe<sub>2</sub>O<sub>3</sub> impregnation—successfully yielded multifunctional composite with promising photocatalytic potential for dye degradation. The utilization of gelatin as a bio-derived template not only improved pore wall integrity but also contributed to a more sustainable and environmentally benign synthesis approach. The sulfonation process under elevated thermal conditions resulted in improved surface acidity functional group density, while incorporation of Fe<sub>2</sub>O<sub>3</sub> endowed the material with enhanced photoresponsivity under visible light irradiation. The observed color transformations and morphological uniformity throughout the synthesis stages suggest a high degree of reproducibility and structural robustness. Future work will focus on detailed physicochemical characterization (e.g., BET surface area, FTIR, XRD, SEM-EDX) and evaluation of photocatalytic performance against methylene blue under visible light, to correlate structural features with catalytic efficacy and assess material stability over multiple degradation cycles.

# 3.6 Synthesis and Impregnation of $Fe_2O_3$ onto Gelatin-Modified Mesoporous Silica

The mesoporous silica material SPG20, known for its high specific surface area and tunable pore architecture, serves as a promising support matrix for the uniform dispersion of active metal oxides, facilitating enhanced surface interactions and catalytic activity. In this study, hematite (Fe<sub>2</sub>O<sub>3</sub>) was employed as the active phase, while gelatin-modified SPG20 acted as the structural and functional support. The synthesis of Fe<sub>2</sub>O<sub>3</sub>/SPG20 was conducted via an ultrasonicassisted impregnation technique. Ultrasonication utilizes high-frequency acoustic waves (>20 kHz) to induce cavitation in liquids, promoting intense localized mixing and preventing agglomeration of metal precursors. This method is increasingly recognized for its eco-friendly, energy-efficient, and selective approach to nanoparticle synthesis, often yielding superior dispersion and particle size control compared to conventional methods such as pyrolysis, hydrothermal treatment, photochemical routes [30]. The impregnation procedure commenced with the dissolution of 0.541 g Fe(Cl)<sub>3</sub>·6H<sub>2</sub>O in 8.9 mL distilled water stirring at 30 °C for 5 minutes. Subsequently, 0.80 g SPG20 was introduced into the solution, and the mixture was subjected to ultrasonication for 2 hours at 30 °C and 100 rpm.

The resulting suspension was oven-dried at  $100\,^{\circ}\mathrm{C}$  for 30 minutes and then calcined at  $600\,^{\circ}\mathrm{C}$  for 6 hours to induce thermal decomposition of precursors and crystallization of the hematite phase [29]. The final product manifested as a bright orange powder with fine textural properties, indicative of successful incorporation of  $\mathrm{Fe_2O_3}$  within the silica matrix.

#### 3.7 X-Ray Diffraction (XRD) Analysis

XRD characterization was employed to determine the crystalline phases, crystallite size, and degree of crystallinity of the samples. Two categories of samples were analyzed: (i) those without metal oxide incorporation, and (ii) Fe<sub>2</sub>O<sub>3</sub>impregnated composites. The XRD patterns of pristine and sulfonated SPG20 (sulfonated at room temperature, 5 °C, 15 °C, and 70 °C) exhibited broad, low-intensity reflections centered around  $2\theta \approx 22^{\circ}$ , characteristic of amorphous silica structures (Figure 5), in accordance with JCPDS 29-0085 [31]. This broad peak indicates a lack of long-range atomic order typical of amorphous silica, consistent with a disordered mesoporous framework that favors high surface area and pore accessibility. The presence of this amorphous background is essential to maintaining structural integrity during subsequent functionalization steps.

In contrast, Fe<sub>2</sub>O<sub>3</sub>-loaded samples such as 20% Fe<sub>2</sub>O<sub>3</sub>/SPG20-SO<sub>3</sub>H prepared at different sulfonation temperatures exhibited distinct reflections at  $2\theta = 24^{\circ}$ ,  $33^{\circ}$ ,  $35^{\circ}$ ,  $40^{\circ}$ ,  $49^{\circ}$ ,  $54^{\circ}$ ,  $62^{\circ}$ , and  $64^{\circ}$ , corresponding to the crystalline hematite

(α-Fe<sub>2</sub>O<sub>3</sub>) phase as referenced in JCPDS 33-0664 [32]. These peaks confirmed the successful formation of crystalline Fe<sub>2</sub>O<sub>3</sub> within the mesoporous matrix. However, samples with lower Fe loading, such as F-20% Fe<sub>2</sub>O<sub>3</sub>/SPG20-SO<sub>3</sub>H (Room) and 1% Fe<sub>2</sub>O<sub>3</sub>/SPG20-SO<sub>3</sub>H (Room), showed no discernible hematite peaks, likely due to insufficient Fe content or the removal of loosely bound species during post-sulfonation washing steps, resulting in either highly dispersed amorphous Fe species or nanocrystallites below the detection threshold of XRD. Crystallite sizes estimated using the Debye-Scherrer equation, and crystallinity percentages were calculated based on the peak broadening. As summarized in Table 1, the highest crystallinity was observed in the pure Fe<sub>2</sub>O<sub>3</sub> sample (90.85%), followed by Fe<sub>2</sub>O<sub>3</sub>-incorporated samples such as  $Fe_2O_3/SPG20-SO_3H(Room)$ , 20% with crystallinity of 80.74%. Notably, crystallinity increased with higher sulfonation temperatures; however, extreme conditions (>70 °C or <5 °C) led to reduced sulfonation efficiency, possibly due to desulfonation or sluggish reaction kinetics, respectively. These findings suggest that room temperature offers an optimal condition for sulfonation, maintaining the amorphous silica framework while enhancing crystallinity. The improved crystallinity is beneficial for increasing thermal and mechanical stability correlated with enhanced photocatalytic performance [33]. Crystalline photocatalysts possess long-range atomic order, which facilitates efficient charge carrier mobility by providing well-

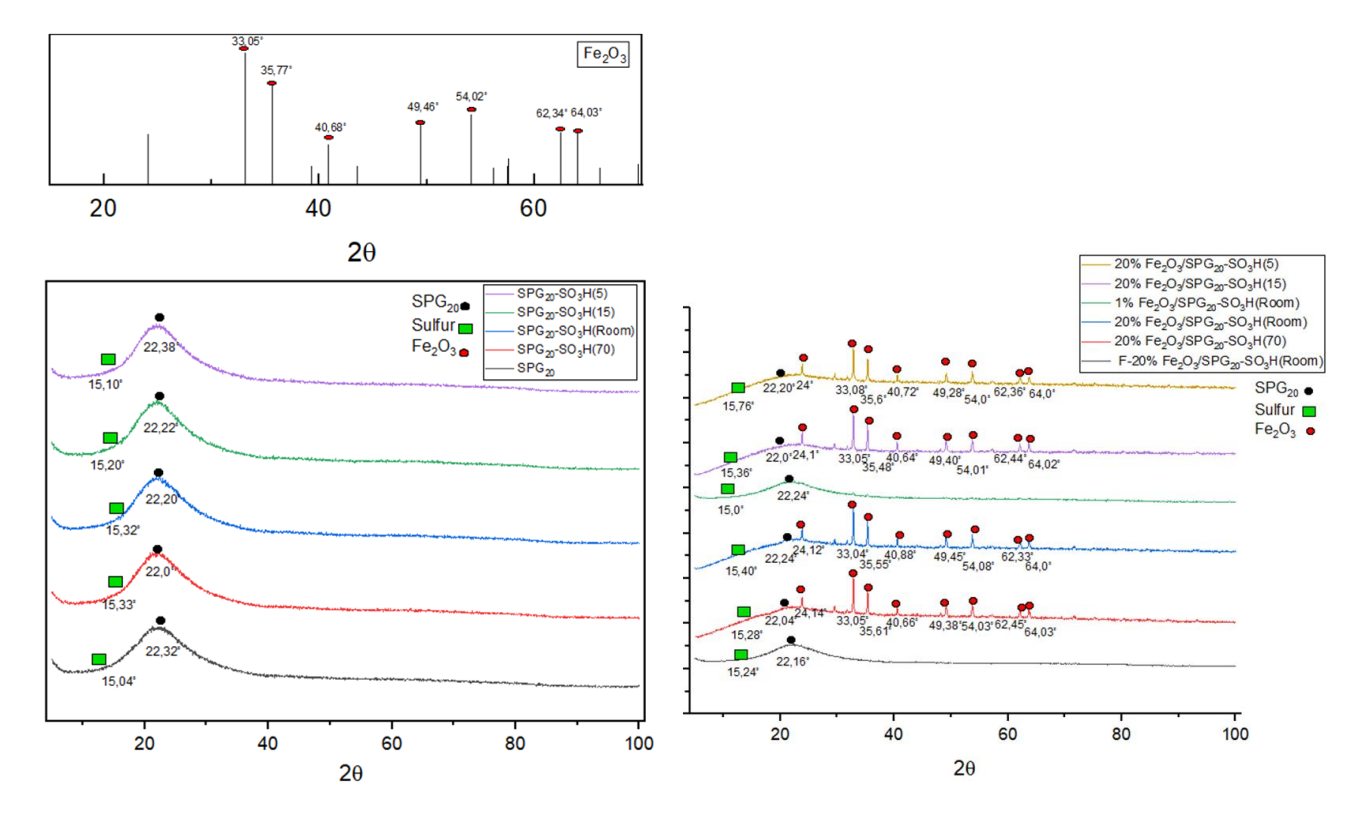


Figure 5. X-Ray Diffraction of SPG20, SPG20-SO<sub>3</sub>H, and Fe<sub>2</sub>O<sub>3</sub>/SPG20-SO<sub>3</sub>H.

defined pathways for electron transport, thus reducing recombination rates. The presence of crystalline α-Fe<sub>2</sub>O<sub>3</sub> within the hybrid matrix plays a pivotal role in light absorption and charge essential factors separation efficiency, photocatalytic activity. Conversely, the amorphous silica support provides a high density of active sites and defects favorable for adsorptive interactions. This unique combination crystalline metal oxide domains dispersed in an amorphous mesoporous silica matrix creates synergistic effects that optimize photocatalytic degradation processes.

Crystalline photocatalysts have long-range atomic order, which results in a well-defined band structure and efficient charge transport pathways. The resulting photocatalytic activity is superior to that of their amorphous counterparts due to the ordered lattice, which minimizes electron-hole recombination [34]. In contrast, amorphous materials lack long-range order, creating a high density of unsaturated coordination sites and defect states. structural disorder widens the band gap and introduces mid-gap states that enhance visible light absorption [35]. Crystalline surfaces offer uniform active sites with specific crystallographic orientations [36]. Amorphous photocatalysts compensate through heterogeneous surface sites [37]. The random atomic arrangement in sulfonated silica-Fe<sub>2</sub>O<sub>3</sub> hybrids creates diverse adsorption pockets for methylene blue, which enhances degradation kinetics. Crystalline photocatalysts dominate in UV-driven systems due to their stability and predictable kinetics [38]. However, amorphous-crystalline composites excel under visible light conditions. Sulfonated silica-Fe<sub>2</sub>O<sub>3</sub> SPG20 hybrid combines the adsorption capacity of amorphous sulfonate groups with the photocatalytic activity of crystalline Fe<sub>2</sub>O<sub>3</sub>, achieving a synergistic degradation rate.

Higher sulfonate group density increases the number of acidic  $-SO_3$  sites on the photocatalyst surface, which strongly attract cationic dyes such blue methylene through electrostatic interactions. This leads to a larger local concentration of dye molecules near the active photocatalytic sites, thus accelerating the degradation rate [39]. Sulfonate groups increase the surface hydrophilicity, facilitating better contact with aqueous dye solutions and enhancing mass transfer. Sulfonate groups can also act as electron transfer sites, enhancing charge separation and reducing recombination, which enhances photocatalytic activity. For example, sulfone-containing polymers have been shown to accelerate electron extraction and enhance hydrogen evolution due to these effects [44,45].

Well-dispersed  $Fe_2O_3$  nanoparticles, as evidenced by the broadening of the XRD peaks,

active provide more accessible sites for photocatalysis. Smaller and more uniformly distributed  $Fe_2O_3$ particles prevent agglomeration, which in turn reduces the surface area and photocatalytic efficiency. The XRD pattern indicating well-crystallized Fe<sub>2</sub>O<sub>3</sub> phase correlates with enhanced visible light absorption and efficient charge carrier generation. Poor crystallinity or large particle aggregates degrade the photocatalytic performance due to increased recombination and reduced active surface area. The combination of well-dispersed Fe<sub>2</sub>O<sub>3</sub> with sulfonated support creates a synergistic effect where Fe<sub>2</sub>O<sub>3</sub> provides photocatalytic sites and sulfonate groups enhance adsorption and charge transfer, which collectively enhance the kinetics of dye degradation.

### 3.8 Fourier Transform Infrared (FTIR) Spectroscopy

FTIR analysis was performed to identify the surface functional groups present in the synthesized materials. All spectra exhibited a broad absorption band in the 3330–3455 cm<sup>-1</sup> region, corresponding to O–H stretching vibrations of surface hydroxyls and adsorbed water (Figure 6). Bending vibrations of adsorbed water molecules appeared near 1617–1638 cm<sup>-1</sup>, while strong Si–O–Si asymmetric and symmetric stretching vibrations were observed in the 1054–1065 cm<sup>-1</sup> region, confirming the presence of siloxane linkages typical of mesoporous silica

Table 1. Crystallite size and degree of crystallinity of SPG20-based materials and their  $\rm Fe_2O_3$  composites.

Sample	D (nm)	Degree of Crystallinity (%)
SPG20	0.92	55.87
$SPG20-SO_3H$ (70 °C)	1.01	56.57
SPG20–SO <sub>3</sub> H (Room Temperature)	0.79	63.55
$SPG20-SO_3H$ (15 °C)	0.97	54.28
$SPG20-SO_3H$ (5 °C)	1.07	58.78
$F-20\%$ $Fe_2O_3/SPG20-SO_3H$ (Room Temperature)	0.83	55.82
20% Fe <sub>2</sub> O <sub>3</sub> /SPG20–SO <sub>3</sub> H (70 °C)	26.18	71.04
$20\% \ Fe_2O_3/SPG20$ – $SO_3H \ (Room \ Temperature)$	1.50	80.74
1% Fe <sub>2</sub> O <sub>3</sub> /SPG20–SO <sub>3</sub> H (Room Temperature)	27.08	58.59
20% $\mathrm{Fe_2O_3/SPG20}\mathrm{-SO_3H}$ (15 °C)	38.78	72.53
20% $\mathrm{Fe_2O_3/SPG20}\mathrm{-SO_3H}$ (5 °C)	1.11	65.03
SPG0	0.99	49.52
Fe <sub>2</sub> O <sub>3</sub> (bulk)	2.14	90.85

frameworks. Following  $Fe_2O_3$  impregnation, new absorption bands emerged around 1620 cm<sup>-1</sup> and below 1000 cm<sup>-1</sup>, which can be attributed to Fe–O stretching vibrations, indicating the successful introduction of iron oxide species onto the silica surface. The intensity of these bands increased proportionally with Fe content, in agreement with the XRD results.

Sulfonation of the silica surface confirmed by the presence of a characteristic S=O stretching band near 1021.12 cm<sup>-1</sup>, corresponding to symmetric and asymmetric vibrations of the -SO<sub>3</sub>H functional group. This peak was absent in the unsulfonated samples and appeared only after sulfonic acid treatment, signifying successful surface modification [42]. These FTIR results provide compelling evidence for the dual functionalization of SPG20: the incorporation of acidic sulfonic groups and transition metal oxide sites. Such bifunctional surface chemistry is highly desirable in heterogeneous catalysis, offering synergistic interactions between Brønsted acid sites and redox-active metal centers.

To further elucidate the spectroscopic findings from a theoretical standpoint, the emergence of Fe–O bands around  $1000~\rm cm^{-1}$  can be theoretically correlated with lattice vibrations of Fe<sub>2</sub>O<sub>3</sub> species interacting with the silica framework. This interaction may involve partial coordination or anchoring of Fe<sup>3+</sup> ions within the silanol-rich mesoporous structure, leading to the formation of stable surface complexes. Such interactions not only confirm the physical presence of iron oxide but also suggest potential electronic effects on the silica support, which could alter the band structure and facilitate charge transfer mechanisms critical in photocatalysis.

The XRD and FTIR characterizations collectively support the superior photocatalytic

performance of  $Fe_2O_3/SPG_{20}$ – $SO_3H$  composites. XRD analysis confirmed the formation of crystalline  $\alpha$ - $Fe_2O_3$  phases, particularly at higher Fe loadings, which contribute to enhanced light absorption and charge carrier separation. The mesoporous silica matrix modified with gelatin preserved structural order, while sulfonation introduced – $SO_3H$  groups, as evidenced by FTIR spectra, enhancing surface acidity and promoting dye adsorption.

Photocatalytic testing (Figure 7) at various temperatures showed that the Fe<sub>2</sub>O<sub>3</sub>/SPG<sub>20</sub>–SO<sub>3</sub>H (70 °C) sample achieved the highest degradation efficiency, reaching 92.14% within 60 minutes. This was followed by the room temperature sample at 89.03%, 15 °C at 86.17%, and 5 °C at 82.76%. These results indicate that elevated temperatures facilitate more efficient dye degradation, likely due to improved charge mobility and increased reaction rates. Notably, all

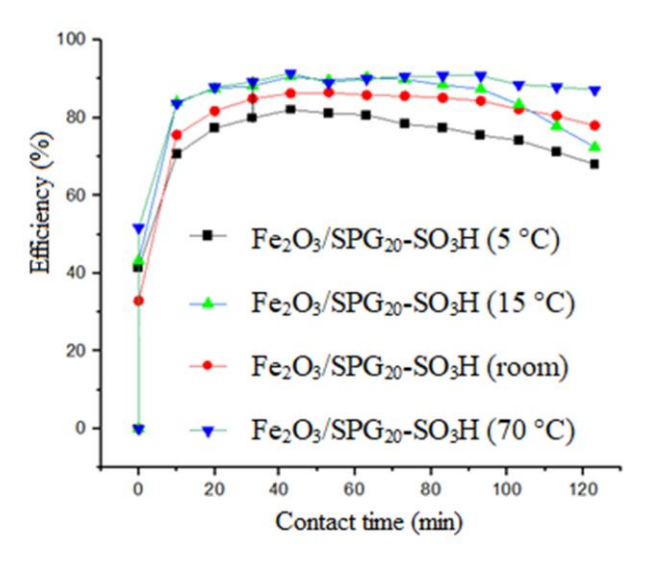


Figure 7. % Efficiency of Fe<sub>2</sub>O<sub>3</sub>/SPG20-SO<sub>3</sub>H.

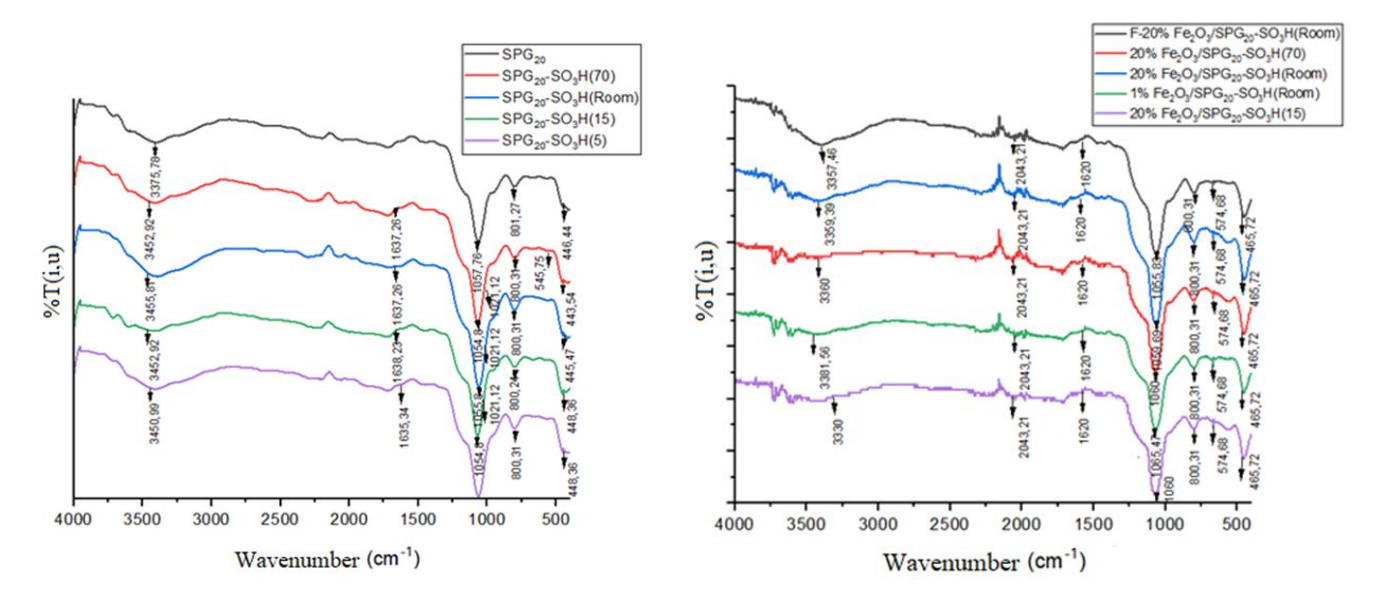


Figure 6. FTIR spectroscopy of SPG20, SPG20-SO<sub>3</sub>H, and Fe<sub>2</sub>O<sub>3</sub>/SPG20-SO<sub>3</sub>H.

samples reached over 80% efficiency, confirming the synergistic effect of mesoporous structure, acidic  $-SO_3H$  groups, and dispersed  $Fe_2O_3$  nanoparticles. The structural and chemical modifications—validated by XRD and FTIR—play a key role in enhancing the photocatalytic degradation of methylene blue under optimized thermal conditions.

The synergistic combination of bifunctional acidity, and metal oxide activity positions this material as a highly promising candidate for advanced photocatalytic applications, particularly in the degradation of organic pollutants such as methylene blue. Fe<sub>2</sub>O<sub>3</sub> (hematite) is a visible-light active semiconductor with a suitable band gap (~2.1 eV) that extends the absorption of light into the visible region, thereby enhancing the photocatalytic efficiency under solar irradiation [43]. Fe<sub>2</sub>O<sub>3</sub> is known to absorb visible light; however, the ultraviolet component of the xenon lamp's broad spectrum also contributes to initiating photocatalytic activity in this system. It should be noted that the use of a relatively lowpower (25 W) xenon lamp may limit the overall light intensity reaching the photocatalyst, potentially resulting in slower degradation rates compared to higher-power sources. Moreover, the mixed UV-visible spectrum of the lamp affects the photocatalytic performance, and future studies employing monochromatic or higher-intensity light sources are recommended to better isolate and understand the photocatalytic mechanisms involved

Loading Fe<sub>2</sub>O<sub>3</sub> onto silica-based materials introduces active sites that can effectively harvest visible light. Sulfonation modifies the electronic environment of the photocatalyst by introducing sulfonic acid groups, which can affect the local permittivity and band edge position [44]. Studies on sulfone-containing polymers have shown that sulfone units enhance the thermodynamic driving force for hole transfer by attracting water molecules, which effectively increases the local permittivity and facilitates oxidation reactions such as oxidation of hole scavengers (e.g., triethylamine) [45]. This can also slightly shift the absorption edge and enhance light harvesting, although the enhancement of intrinsic optical absorption is moderate compared to the overall activity enhancement. The sulfonic acid groups introduced through sulfonation provide acidic functional sites that enhance the absorption of cationic dyes such as methylene blue through electrostatic interactions [46]. This enhanced adsorption near the photocatalytic concentrates the pollutant molecules, enhancing the degradation kinetics. The sulfonated surface increases the hydrophilicity ofphotocatalyst, enhancing the interaction with the aqueous medium and reactants, which is critical for effective photocatalysis [47].

 $Fe_2O_3$ nanoparticles serve as active photocatalytic centers where photogenerated electrons and holes participate in redox reactions. However, Fe<sub>2</sub>O<sub>3</sub> itself often undergoes rapid charge recombination. The presence of sulfonate groups can facilitate faster electron extraction and hole transfer by acting as electron transfer sites, thereby increasing  $_{
m the}$ charge separation efficiency. Sulfonation enhances the electron transfer kinetics from the photocatalyst to the cocatalyst or electron acceptor, as demonstrated by sulfone-containing polymers where sulfone units act as electron transfer sites, accelerating electron extraction and thereby enhancing photocatalytic hydrogen evolution. The combined effects of Fe<sub>2</sub>O<sub>3</sub> loading and sulfonation create a synergistic pathway for efficient charge separation and transfer, reducing recombination losses and enhancing photocatalytic activity.

From theoretical a perspective, integration of sulfonic acid groups and Fe<sub>2</sub>O<sub>3</sub> nanoparticles within the mesoporous silica framework creates a multifunctional hybrid system with synergistic properties. The sulfonate groups act as electron-withdrawing moieties, which can lower the conduction band edge and increase the separation potential photogenerated Meanwhile, charges.  $Fe_2O_3$ introduces mid-gap states that enable visible-light absorption and facilitate electron excitation. The electron density redistribution between these functional groups and the silica framework modifies the local electronic environment, which favorable for redox reactions on the photocatalyst surface.

The proposed photocatalytic mechanism for methylene blue degradation by sulfonated SPG20 silica-Fe<sub>2</sub>O<sub>3</sub> hybrid photocatalysts is briefly that when the photocatalyst is irradiated with light with sufficient energy (≥ bandgap), electrons are excited from the valence band (VB) to the conduction band (CB), leaving positive holes in the VB. This process produces chemically active electron-hole pairs. Although DFT calculations were not performed in this study, previous theoretical investigations have shown that the internal electric field at the interface of metal oxides and sulfonated silica can enhance charge separation. For instance, DFT-based simulations on related hybrid materials have demonstrated that electron-withdrawing -SO<sub>3</sub>H groups and interfacial heterojunctions facilitate directional charge transport and suppress charge recombination [48]. These insights theoretical support to explain the observed enhancement in photocatalytic activity in our system:

Photocatalyst + 
$$hv \rightarrow e_{CB^-} + h_{VB^+}$$
 (1)

The electrons in the conduction band react with dissolved oxygen to form superoxide anion radicals ( $\cdot$ O<sub>2</sub> $\cdot$ ). The positive holes in the valence band oxidize water or hydroxide ions to form hydroxyl radicals ( $\cdot$ OH), which are strong oxidizing species:

$$O_2 + e_{CB^-} \rightarrow \cdot O_2^- \tag{2}$$

$$H_2O + h_{VB}^+ \rightarrow \cdot OH + H^+$$
 (3)

The results presented in Table 2 provide compelling evidence that low-temperature sulfonation is capable of producing sulfonated materials with structural and functional characteristics comparable to those synthesized at higher temperatures. Previous studies employing sulfonation temperatures between 80 °C and served as 160 °C critical references understanding the role of temperature in developing mesostructural order, active -SO<sub>3</sub>H group formation, and thermal stability. In the present work, sulfonation conducted significantly lower temperatures (5, 15, room temperature, and 70 °C) yielded materials with strong Brønsted acidity, efficient sulfonic acid functionalization, and favorable mesoporous characteristics. Notably, sulfonation temperature plays a crucial role in enhancing photocatalytic performance. The presence of -SO<sub>3</sub>H groups on the photocatalyst surface enhances the adsorption of methylene blue molecules via electrostatic attraction between the negatively charged sulfonate groups and the cationic dye. Improved adsorption increases the local concentration of pollutants near the active sites, thereby accelerating the photocatalytic degradation process. Moreover, functionalization improves the hydrophilicity of the catalyst surface, promoting better interaction with water and dissolved oxygen.

interactions facilitate the generation of reactive species such as hydroxyl and superoxide radicals, which effectively break down methylene blue into non-toxic end products like  $CO_2$ ,  $H_2O$ , and sulfate ions. Collectively, these findings confirm that energy-efficient, low-temperature sulfonation not only preserves material integrity but also supports environmentally friendly and high-performance photocatalysis.

The results presented in Table 1 provide strong evidence that low-temperature sulfonation is capable of producing sulfonated materials with competitive structural and chemical properties compared to those synthesized at higher temperatures. Prior studies, which utilized sulfonation temperatures ranging from 80 °C to 160 °C, served as essential benchmarks for evaluating the effect of temperature on the formation of active -SO<sub>3</sub>H groups, structural stability, and surface characteristics. In contrast, the present study successfully demonstrates that sulfonation at significantly lower temperatures (5, 15, room temperature, and 70 °C) yields materials with desirable mesostructural integrity, strong acidity, and effective sulfonic functionalization. These findings underscore the potential of energyefficient sulfonation strategies to generate functional catalytic materials without compromising performance, thereby promoting greener and more sustainable synthesis pathways.

The  $Fe_2O_3/Silica$  SPG-20– $SO_3H$  sample synthesized in this study demonstrates above-average characteristics compared to previously reported materials (Table 3). With a high surface area and strong Brønsted acidity, this catalyst achieves a relatively high methylene blue photodegradation efficiency of 92.12% within 120 minutes, outperforming many other photocatalysts such as  $Nb_2O_2-H_2O_2$  (45.2%) and

Table 2. Comparison of sulfonated materials character in different temperatu	re.
--	-----

No Sample Name		Sulfonation Temperature (°C)	Dominant Characteristics	Reference	
1	Carbon coal tar pitch $-SO_3H$	160	High thermal stability, disordered mesoporous pores	[49]	
2	Polymer PGMA–SO <sub>3</sub> H	80	regulerl structure, sulfonate groups formed	[50]	
3	isoleucine doped Creatininium–SO <sub>3</sub> H	32	Active $-SO_3H$ groups, low crystallinity	[51]	
4	$SiO_2$ – $SO_3H$	120	Well-dispersed Fe, high photocatalytic activity	[52]	
5	MWCNT-SO <sub>3</sub> H	80	Stable mesoporous structure, active sulfonate groups	[53]	
6	Carbon-SO <sub>3</sub> H	80	Strong Brønsted acidity, large surface area	[54]	
7	$Fe_2O_3/SPG_{20}$ – $SO_3H$	5-70	$\alpha$ -Fe <sub>2</sub> O <sub>3</sub> crystals, active -SO <sub>3</sub> H	This work	

TiO<sub>2</sub>/SBA-15 (67.5%). This superior performance indicates that the combination of sulfonation and iron oxide impregnation effectively enhances the material's photocatalytic activity.

The results highlight the critical role of sulfonation when combined with metal impregnation on mesoporous silica synthesized using gelatin as a dual template. The gelatin template contributes to improved pore structure and stability, while sulfonic acid groups introduce strong acidity and increased adsorption sites, facilitating efficient interaction between the catalyst surface and methylene blue molecules. Together, these factors synergistically promote enhanced photocatalytic degradation. demonstrating a promising approach developing effective and environmentally friendly catalysts for dye-contaminated wastewater treatment. Surface area plays a crucial role in the photocatalytic activity of materials, as it directly influences the availability of active sites for adsorption and reaction. From the BET surface area data reported in previous studies, it can be estimated that the Fe<sub>2</sub>O<sub>3</sub>/sulfonated silica materials typically exhibit surface areas in the range of 200-400 m²/g. Although the exact BET surface area for the Fe<sub>2</sub>O<sub>3</sub>/Silica SPG20–SO<sub>3</sub>H catalyst in this work was not determined due to experimental constraints, this estimated range provides a reasonable baseline. This inference supports the understanding that photocatalytic efficiency is not solely governed by the presence of metal active sites but is also significantly

enhanced by additional functional groups such as sulfonic acid (-SO<sub>3</sub>H) introduced via sulfonation, as well as the inherent high surface area of the mesoporous support. Together, these factors synergistically improve adsorption, separation, and overall catalytic performance, emphasizing the importance of both chemical functionality and physical structure in designing effective photocatalysts. Together, these factors synergistically improve adsorption, charge separation, and overall catalytic performance, emphasizing the importance of both chemical functionality and physical structure in designing effective photocatalysts. Further investigations are planned to assess the reusability and structural stability of the Fe<sub>2</sub>O<sub>3</sub>/SPG20-SO<sub>3</sub>H catalyst under multiple photocatalytic cycles, which are critical parameters for determining its practical applicability and long-term operational performance. Moreover, the straightforward use synthesis method and of low-cost. biocompatible templating agents suggest a promising potential for industrial scalability and implementation practical large-scale wastewater treatment systems.

As shown in Figures 8-9 and Table 4, SEM images clearly display morphological differences where the post-photocatalysis sample exhibits denser agglomeration, suggesting possible restructuring or surface reconstruction during photocatalytic activity. Furthermore. elemental mapping and quantification data reveal the elemental changes in composition,

Table 3. Comparative photocatalytic performance of photodegradation methylene blue materials.

No	Sample Name	Characteristics	$S_{BET}(m^2/g)$	% Photodegradation	Reference
1	Nb <sub>2</sub> O <sub>2</sub> -H <sub>2</sub> O <sub>2</sub>	Stable structure, high surface acidity	75.4	45.2% (90 min)	[55]
2	TiO2/SBA-15	Hexagonal structure, good thermal stability	384.2	67.5% (90 min)	[56]
3	Cu/TiO <sub>2</sub>	Well-dispersed Cu, strong photocatalytic activity	30.0	32.4% (60 min)	[57]
4	P125	Amorphous structure	50.0	38.0% (60 min)	[58]
5	ZnO-silica-SO <sub>3</sub> H	mesopores, gelatin- enhanced stability	425.7	97.6% (90 min)	[17]
6	Fe <sub>2</sub> O <sub>3</sub> /Silica SPG20–SO <sub>3</sub> H	High surface area, strong Brønsted acidity	ND	92.12% (120 min)	This work

Table 4. Element analysis of Fe<sub>2</sub>O<sub>3</sub>/SPG20-SO<sub>3</sub>H-70 °C before and after photocatalysis.

Sample	Elemental %wt.					
	C	О	Si	Fe	S	Others
Before Photocatalysis	2.81	50.31	40.11	5.35	2.10	0.68
After Photocatalysis	7.74	42.54	41.21	5.39	2.21	0.91

particularly increases in C and S content, potentially attributed to adsorbed intermediates or partial organic residue deposition during methylene blue degradation. These results indicate not only the physical transformation of the photocatalyst but also the interaction with reactants during the process.

Moreover, FTIR spectra (Figure 10) show significant variation in transmittance bands before and after photocatalysis, particularly in the region associated with Fe–O, Si–O–Si, and  $SO_3H$  functional groups, supporting the hypothesis of surface interaction and partial structural modification during photocatalytic action.

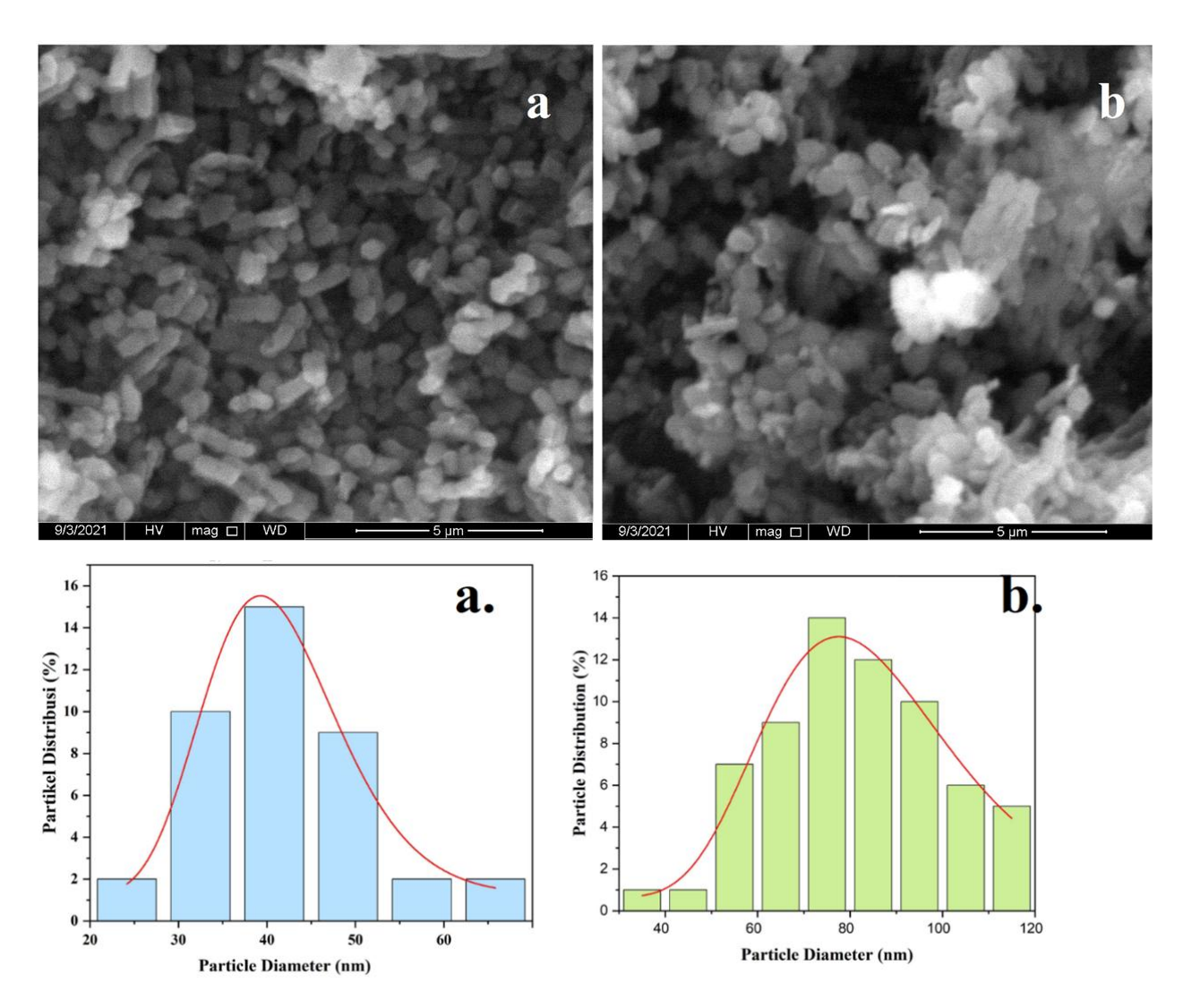


Figure 8. Morphology, particle distribution and of  $Fe_2O_3/SPG20-SO_3H$  (70 °C) a. before and b. after photocatalysis

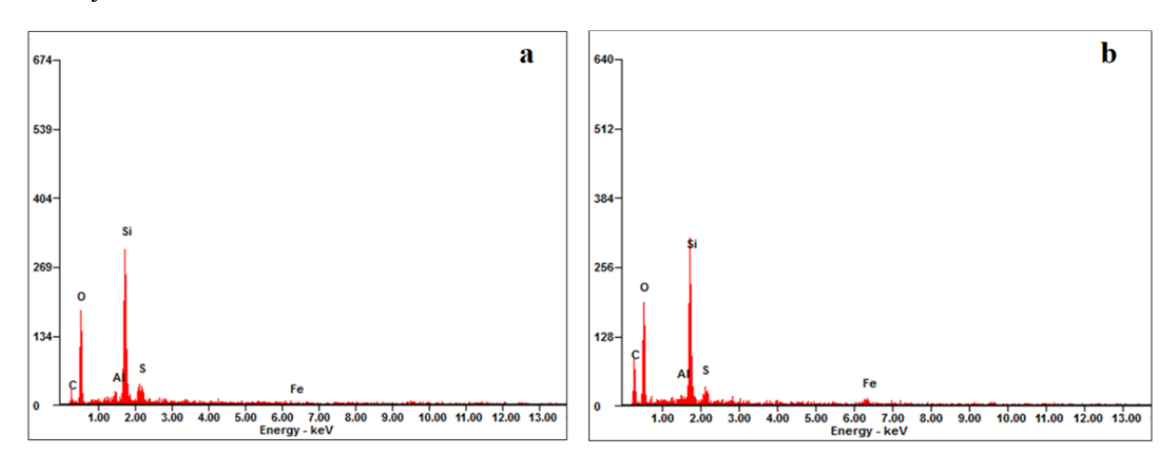


Figure 9. Elemental composition by SEM-EDX of  $Fe_2O_3/SPG20$ -SO<sub>3</sub>H (70 °C) a. before and b. after photocatalysis.

Altogether, these comprehensive characterizations validate the structural integrity, reactivity, and photocatalytic activity of the synthesized material under operational conditions.

In addition, UV-Vis DRS analysis (Figure 11) was performed to evaluate the light absorption properties and estimate the band gap energy of Fe<sub>2</sub>O<sub>3</sub>/SPG20-SO<sub>3</sub>H, which is essential for assessing its photocatalytic potential. The band gap changes before and after thermal treatment suggest enhanced visible light absorption attributed to structural integration of Fe species and sulfonic groups. The thermal treatment during the sulfonation process significantly influences the optical band gap of the Fe<sub>2</sub>O<sub>3</sub>/SPG20-SO<sub>3</sub>H photocatalyst, as evidenced in the UV-Vis DRS Tauc plots. Among the samples treated at different temperatures (15 °C, room temperature, and 70 °C), the material sulfonated at 70 °C exhibited the lowest band gap energy, indicating enhanced visible light absorption. This reduction in band gap is attributed to improved structural ordering and electron delocalization induced by the optimal thermal activation at 70 °C. The elevated temperature likely promotes stronger interaction between Fe<sub>2</sub>O<sub>3</sub> particles and the sulfonated silica matrix, leading to better integration and charge transfer efficiency. In contrast, lower sulfonation temperatures (15 °C and room temperature) result in wider band gaps, suggesting less effective incorporation functional groups and weaker interaction between the active sites and the support. Thus, 70 °C is considered the optimal sulfonation temperature for achieving superior photocatalytic performance due to its ability to generate a more responsive structure under visible light.

The combination of morphological, compositional, structural, and optical analyses

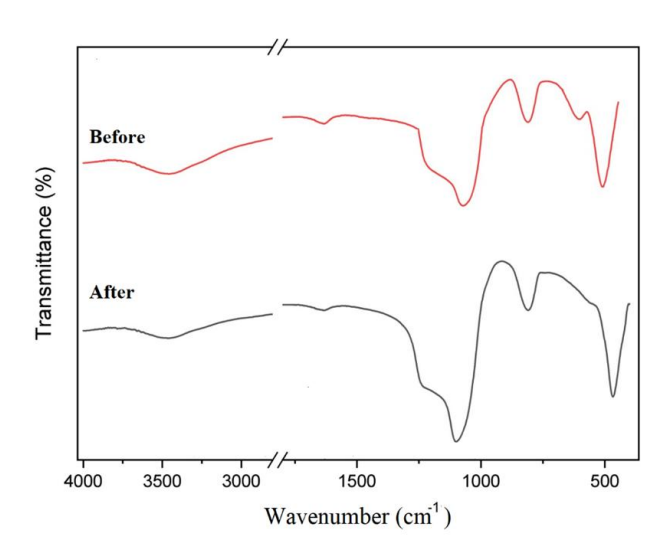


Figure 10. FTIR spectra of Fe $_2\rm O_3/SPG20\text{-}SO_3H$  (70 °C) a. before and b. after photocatalysis.

synthesized strongly confirms that the Fe<sub>2</sub>O<sub>3</sub>/SPG20-SO<sub>3</sub>H photocatalyst undergoes significant structural evolution and surface interaction during photocatalytic activity. The observed improvements in particle integration, band gap narrowing, and functional group stability—particularly in the sample sulfonated at 70 °C—highlight the crucial role of thermal treatment in optimizing photocatalyst performance. These findings not only validate the material's photocatalytic potential but also the importance of underscore controlled sulfonation temperature in designing efficient, stable, and visible-light-responsive photocatalysts for environmental applications.

#### 4. Conclusion

This study successfully developed a novel Fe<sub>2</sub>O<sub>3</sub>-impregnated mesoporous silica (SPG20) photocatalyst modified with gelatin and sulfonic acid groups. The synthesis approach utilized an environmentally friendly, template-assisted route involving ultrasonication to enhance the uniform dispersion of Fe<sub>3</sub><sup>+</sup> species across the mesoporous network. The resulting material demonstrated a of high degree structural integrity, multifunctionality, and potential environmental photocatalysis. Among all variants, the 20% Fe<sub>2</sub>O<sub>3</sub>/SPG20-SO<sub>3</sub>H sample prepared at ambient conditions exhibited the most favorable physicochemical characteristics. including high crystallinity, strong functionalization, and potential for large-scale applicability in wastewater treatment. Overall, the integrated design of Fe<sub>2</sub>O<sub>3</sub> and -SO<sub>3</sub>H within a mesoporous framework presents a sustainable and efficient photocatalytic system. The use of a 25 W UV-visible xenon lamp proved sufficient to initiate photocatalytic degradation, despite the light source spectrum not being exclusively within

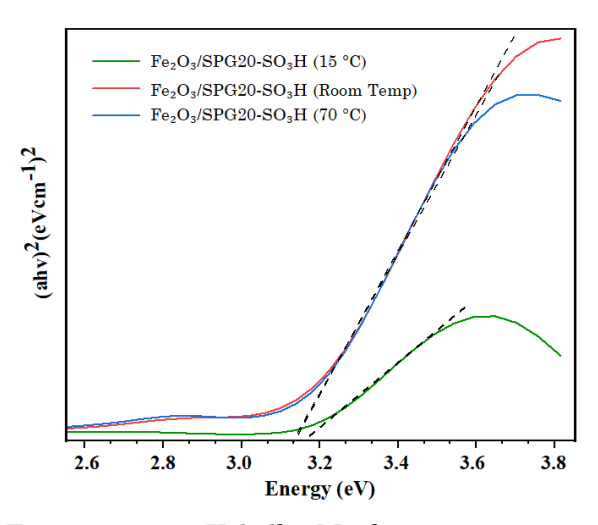


Figure 11. Kobelka-Menk representation. (F(R)hv)2 with Energy in UV-vis spectrum  $Fe_2O_3/SPG20-SO_3H$ .

the visible range. Further studies employing more specific and controlled light spectra are recommended to fully elucidate the photocatalytic mechanisms of  $Fe_2O_3$ . This research contributes to the advancement of multifunctional materials for dye degradation and supports further exploration in environmental remediation technologies. Future studies should explore kinetic parameters, photodegradation pathways, and catalyst reusability to fully exploit the material's performance in real-world applications.

#### Acknowledgments

The authors would like to express their sincere gratitude to Universitas Sebelas Maret (UNS) for the financial support provided through the Penelitian Unggulan Terapan A (PUTA-UNS) research grant scheme, under contract number 369/UN27.22/PT.01.03/2025. This funding has been pivotal in enabling the successful completion of this research. We also extend our appreciation to all those who have contributed their expertise, resources, and time towards this study, making it possible to explore and develop the innovative solutions presented in this work.

#### **CRedit Author Statement**

Ulfa: Author Contributions: M. Conceptualization, Investigation, Resources, Data Curation, Writing, Review and Editing, Supervision; M. Ulfa and P.R. Salsabila: Methodology, Formal Analysis, Data Curation, Writing Draft Preparation; M. Ulfa: Review and Editing, Data Curation M. Ulfa and P.R. Salsabila and Validation M. Ulfa, P.R. Salsabila, A.N.C. Saputro and N.D.Nurhayati. All authors have read and agreed to the published version of the manuscript.

#### References

- [1] Patwari, S.S., Elections, G. (2024). Texprocil. VII(1).
- [2] Ardrarani, G., Rachmawati, L. (2023). Pengaruh Kualitas Produk, Harga dan Keputusan Pembelian Pakaian Bekas Thrifting. Journal of Economics, 3(2), 42–52. DOI: 10.26740/independent.v3n1.p42-52
- [3] Lellis, B., Fávaro-Polonio, C.Z., Pamphile, J.A., Polonio, J.C. (2019). Effects of textile dyes on health and the environment and bioremediation potential of living organisms. *Biotechnology Research and Innovation*, 3(2), 275–290. DOI: 10.1016/j.biori.2019.09.001.
- [4] Islam, M., Rakha, A., Nawaj, J., Mondal, H. (2025). A critical review on textile dye-containing wastewater: Ecotoxicity, health risks, and remediation strategies for environmental safety. Cleaner Chemical Engineering, 11(January), 100165. DOI: 10.1016/j.clce.2025.100165.

- [5] Sarkar Phyllis, A.K., Tortora, G., Johnson, I.
   (2022). Photodegradation. Fairchild Books Dict Text. DOI: 10.5040/9781501365072.12105
- [6] Chahal, M., Kumari, S., Bhattacharya, A., Garg, M.C. (2024). Evaluating sustainable agricultural waste biomass for methylene blue adsorption in wastewater treatment: A state-of-the-art review. Bioresource Technology Reports, 28(May), 101983. DOI: 10.1016/j.biteb.2024.101983.
- [7] Liu, Y., Chen, J., Duan, D., Zhang, Z., Liu, C., Cai, W., Zhao, Z. (2024). Environmental Impacts and Biological Technologies Toward Sustainable Treatment of Textile Dyeing Wastewater: A Review. Sustainability (Switzerland), 16(24) DOI: 10.3390/su162410867.
- [8] Bopape, D.A., Ntsendwana, B., Mabasa, F.D. (2024). Photocatalysis as a pre-discharge treatment to improve the effect of textile dyes on human health: A critical review. *Heliyon*, 10(20), e39316. DOI: 10.1016/j.heliyon.2024.e39316.
- [9] Obayomi, O.V., Olawoyin, D.C., Oguntimehin, O., Mustapha, L.S., Kolade, S.O., Oladoye, P.O., Oh, S., Obayomi, K.S. (2024). Exploring emerging water treatment technologies for the removal of microbial pathogens. *Current Research in Biotechnology*, 8(May). DOI: 10.1016/j.crbiot.2024.100252.
- [10] Kainth, S., Sharma, P., Pandey, O.P. (2024). Green sorbents from agricultural wastes: A review of sustainable adsorption materials. Applied Surface Science Advances, 19(September 2023), 100562. DOI: 10.1016/j.apsadv.2023.100562.
- [11] Oyewo, O.A., Muliwa, A.M., Makgato, S.S., Onwudiwe, D.C. (2025). Research progress on green adsorption process for water pollution control applications. *Hybrid Advances*, 8(September 2024), 100338. DOI: 10.1016/j.hybadv.2024.100338.
- [12] Oladoye, P.O., Kadhom, M., Khan, I., Hama Aziz, K.H., Alli, Y.A. (2024). Advancements in adsorption and photodegradation technologies for Rhodamine B dye wastewater treatment: fundamentals, applications, and future directions. *Green Chemical Engineering*, 5(4), 440–460. DOI: 10.1016/i.gce.2023.12.004.
- [13] Mohd Adnan, M.A., Bao, L.P., Muhd Julkapli, N. (2020). Mitigation of pollutants by chitosan/metallic oxide photocatalyst: A review. *Journal of Cleaner Production*, 261, 121190. DOI: 10.1016/j.jclepro.2020.121190.
- [14] Hakim, A.L., Sari, I.E., Nur Sabrina, B.J., Nurkhalizah, Z.A., Ajeng Zahabiya, E.K., Hidayat, A.N., Sulistiono, D.O., Sopiah, R.N., Kusumawati, Y., Ediati, R. (2025). Impregnation of porous TiO2/ZnO into MCM-41 synthesized from coal fly ash for enhanced photocatalytic activity of TiO2/ZnO@MCM-41 composites in methylene blue removal. Case Studies in Chemical and Environmental Engineering, 11(December 2024), 101152. DOI: 10.1016/j.cscee.2025.101152.

- [15] Ahmad Hariza, A.M., Mohd Yunus, M.H., Fauzi, M.B., Murthy, J.K., Tabata, Y., Hiraoka, Y. (2023). The Fabrication of Gelatin–Elastin– Nanocellulose Composite Bioscaffold as a Potential Acellular Skin Substitute. *Polymers*, 15(3). DOI: 10.3390/polym15030779.
- [16] Cheng, J., Gao, R., Zhu, Y., Lin, Q. (2024). Applications of biodegradable materials in food packaging: A review. Alexandria Engineering Journal, 91(January), 70–83. DOI: 10.1016/j.aej.2024.01.080.
- [17] Ulfa, M., Aziza, H., Sholeha, N.A. (2025). In-situ sulfonated mesoporous silica as ZnO nanomaterial support for enhanced dyes photodegradation. Results in Engineering, 26(February), 104381. DOI: 10.1016/j.rineng.2025.104381.
- [18] Xie, T., Zeng, C., Wang, C., Zhang, L. (2013). Preparation of methyl ester sulfonates based on sulfonation in a falling film microreactor from hydrogenated palm oil methyl esters with gaseous SO3. *Industrial and Engineering Chemistry Research*, 52(10), 3714–3722. DOI: 10.1021/ie3028763.
- [19] Qadariyah, L., Sahila, S., Mahfud, M. (2021). The effect of reaction time and temperature on the synthesis of methyl ester sulfonate surfactant from palm oil as a feedstock using microwave-assisted heating. ASEAN Journal of Chemical Engineering, 21(1), 104–112. DOI: 10.22146/ajche.63786.
- [20] Mandal, S., Adhikari, S., Pu, S., Wang, X., Kim, D.H., Patel, R.K. (2019).Interactive Fe2O3/porous SiO2 nanospheres for photocatalytic degradation of organic pollutants: approach. Kinetic and mechanistic Chemosphere, 234, 596-607. DOI: 10.1016/j.chemosphere.2019.06.092.
- [21] Abhishek B., Jayarama A., Rao, A.S., Nagarkar, S.S., Dutta, A., Duttagupta, S.P., Prabhu, S.S., Pinto, R. (2024). Challenges in photocatalytic hydrogen evolution: Importance of photocatalysts and photocatalytic reactors. International Journal of Hydrogen Energy, 81(July), 1442–1466. DOI: 10.1016/j.ijhydene.2024.07.262.
- [22] Ulfa, M., Nina, Pangestuti, I., Holilah, Bahruji, H., Rilda, Y., Alias, S.H., Nur, H. (2024). Enhancing photocatalytic activity of Fe2O3/TiO2 with gelatin: A fuzzy logic analysis of mesoporosity and iron loading. South African Journal of Chemical Engineering, 50(August), 245–260. DOI: 10.1016/j.sajce.2024.08.011.
- [23] Ulfa, M., Prasetyoko, D., Mahadi, A.H., Bahruji, H. (2020). Size tunable mesoporous carbon microspheres using Pluronic F127 and gelatin as co-template for removal of ibuprofen. Science of the Total Environment, 711, 135066. DOI: 10.1016/j.scitotenv.2019.135066.

- [24] Ulfa, M., Iswanti, Y., Irwanti, Y., Sholeha, N.A., Masruchin, N., Subagyo, R., Bahruji, H., Prasetyoko, D. (2023). Hydrothermal effect of gunningite use Pluronic F127-Gelatin as template and the ibuprofen adsorption performance. *Heliyon*, 9(3), e14473. DOI: 10.1016/j.heliyon.2023.e14473.
- [25] Liang, S., Zhang, J., Huang, S., Lan, X., Wang, W., Tang, Y. (2025). Functionalized Gelatin Electrospun Nanofibrous Membranes in Food Packaging: Modification Strategies for Fulfilling Evolving Functional Requirements. *Polymers*, 17(8), 1–32. DOI: 10.3390/polym17081066.
- [26] Komadel, P., Madejová, J. (2013). Acid activation of clay minerals, 2nd ed. Elsevier Ltd.
- [27] Zailan, Z., Tahir, M., Jusoh, M., Zakaria, Z.Y. (2021). A review of sulfonic group bearing porous carbon catalyst for biodiesel production. Renewable Energy, 175, 430–452. DOI: 10.1016/j.renene.2021.05.030.
- [28] Toy, M., Recepoğlu, Y.K., Arar, Ö. (2025).
  Sulfonated Cellulose: A Strategy for Effective
  Methylene Blue Sequestration. ACS Omega.
  10(8), 8696–8708. DOI:
  10.1021/acsomega.5c00179
- [29] Munnik, P., De Jongh, P.E., De Jong, K.P. (2015). Recent Developments in the Synthesis of Supported Catalysts. Chemical Reviews, 115(14), 6687–6718. DOI: 10.1021/cr500486u.
- [30] Gong, X., Jadhav, N.D., Lonikar, V. V., Kulkarni, A.N., Zhang, H., Sankapal, B.R., Ren, J., Xu, B. Bin, Pathan, H.M., Ma, Y., Lin, Z., Witherspoon, E., Wang, Z., Guo, Z. (2024). An overview of green synthesized silver nanoparticles towards bioactive antibacterial, antimicrobial and antifungal applications. Advances in Colloid and Interface Science, 323(November 2023), 103053. DOI: 10.1016/j.cis.2023.103053.
- [31] Huang, S., Ma, P., Wei, Y., Cheng, Z., Liu, B., Deng, X., Xie, Z., Xing, B., Lin, J. (2020). Controllable synthesis of hollow porous silica nanotubes/CuS nanoplatform for targeted chemo-photothermal therapy. Science China Materials, 63(5), 864–875. DOI: 10.1007/s40843-019-1235-1.
- [32] Liu, L., Fu, S., Lv, X., Yue, L., Fan, L., Yu, H., Gao, X., Zhu, W., Zhang, W., Li, X., Zhu, W. (2020). A Gas Sensor With Fe2O3 Nanospheres Based on Trimethylamine Detection for the Rapid Assessment of Spoilage Degree in Fish. Frontiers in Bioengineering and Biotechnology, 8(September), 1–9. DOI: 10.3389/fbioe.2020.567584.
- [33] Mao, T., Zha, J., Hu, Y., Chen, Q., Zhang, J., Luo, X. (2024). Research Progress of TiO2 Modification and Photodegradation of Organic Pollutants. *Inorganics*, 12(7) DOI: 10.3390/inorganics12070178.

- [34] Islam, A., Malek, A., Islam, M.T., Nipa, F.Y., Raihan, O., Mahmud, H., Uddin, M.E., Ibrahim, M.L., Abdulkareem-Alsultan, G., Mondal, A.H., Hasan, M.M., Salman, M.S., Kubra, K.T., Hasan, M.N., Sheikh, M.C., Uchida, T., Rasee, A.I., Rehan, A.I., Awual, M.E., Hossain, M.S., Waliullah, R.M., Awual, M.R. (2025). Next frontier in photocatalytic hydrogen production through CdS heterojunctions. *International Journal of Hydrogen Energy*, 101(November 2024), 173–211. DOI: 10.1016/j.ijhydene.2024.12.300.
- [35] Zafar, Z., Yi, S., Li, J., Li, C., Zhu, Y., Zada, A., Yao, W., Liu, Z., Yue, X. (2022). Recent Development in Defects Engineered Photocatalysts: of Overview An the Experimental and Theoretical Strategies. Energy and Environmental Materials, 5(1), 68-114. DOI: 10.1002/eem2.12171.
- [36] Qi, Z., Xi, M., Liu, Z., Sheng, R., Wang, W., Wu, T., Huang, Y. (2024). Preferred crystal surface exposure and near-crystal surface desolvation construct efficient Zn plating/stripping reversibility. Chemical Engineering Journal, 499 (July), 156228. DOI: 10.1016/j.cej.2024.156228.
- [37] Sun, Z., Bai, C., Zheng, S., Yang, X., Frost, R.L. (2013). A comparative study of different porous amorphous silica minerals supported TiO2 catalysts. *Applied Catalysis A: General*, 458, 103–110. DOI: 10.1016/j.apcata.2013.03.035.
- [38] Tsaviv, J.N., Eneji, I.S., Shato'Ato, R., Ahemen, I., Jubu, P.R., Yusof, Y. (2024). Photodegradation, kinetics and non-linear error functions of methylene blue dye using SrZrO3 perovskite photocatalyst. *Heliyon*, 10(14). DOI: 10.1016/j.heliyon.2024.e34517.
- [39] Mills, A., Sheik, M., O'Rourke, C., McFarlane, M. Adsorption and photocatalysed destruction of cationic and anionic dyes on mesoporous titania films: Reactions at the airsolid Appliedinterface. Catalysis B: 89(1-2),DOI: Environmental, 189–195. 10.1016/j.apcatb.2008.11.029.
- [40] Li, X., Chen, Y., Tao, Y., Shen, L., Xu, Z., Bian, Z., Li, H. (2022). Challenges of photocatalysis and their coping strategies. *Chem Catalysis*, 2(6), 1315–1345. DOI: 10.1016/j.checat.2022.04.007.
- [41] Li, A., Zhang, P., Kan, E., Gong, J. (2024). Wettability adjustment to enhance mass transfer for heterogeneous electrocatalysis and photocatalysis. *eScience*, 4(1), 100157. DOI: 10.1016/j.esci.2023.100157.
- [42] Moein Najafabadi, S., Safaei Ghomi, J. (2023). Synthesis of COF-SO3H Immobilized on Manganese Ferrite Nanoparticles As An Efficient Nanocomposite in The Preparation of spirooxindoles. *Scientific Reports*, 13(1). DOI: 10.1038/s41598-023-49628-7.

- [43] Kumar, Y., Kumar, R., Raizada, P., Khan, A.A.P., Singh, A., Le, Q. Van, Nguyen, V.H., Selvasembian, R., Thakur, S., Singh, P. (2022). Current status of hematite (α-Fe2O3) based Z-scheme photocatalytic systems for environmental and energy applications. Journal of Environmental Chemical Engineering, 10(3), 107427. DOI: 10.1016/j.jece.2022.107427.
- [44] Dostanić, J., Lončarević, D., Hadnađev-Kostić, M., Vulić, T. (2024). Recent Advances in the Strategies for Developing and Modifying Photocatalytic Materials for Wastewater Treatment. *Processes*, 12(9), 1914. DOI: 10.3390/pr12091914.
- [45] Hillman, S.A.J., Sprick, R.S., Pearce, D., Woods, D.J., Sit, W.Y., Shi, X., Cooper, A.I., Durrant, J.R., Nelson, J. (2022). Why Do Sulfone-Containing Polymer Photocatalysts Work so Well for Sacrificial Hydrogen Evolution from Water? Journal of the American Chemical Society, 144(42), 19382–19395. DOI: 10.1021/jacs.2c07103.
- [46] Li, J., Li, H., Yuan, Z., Fang, J., Chang, L., Zhang, H., Li, C. (2019). Role of sulfonation in lignin-based material for adsorption removal of cationic dyes. *International Journal of Biological Macromolecules*, 135, 1171–1181. DOI: 10.1016/j.ijbiomac.2019.06.024.
- [47]Lee, D.E., Kim, M.K., Danish, M., Jo, W.K. (2023). State-of-the-art review on photocatalysis for efficient wastewater treatment: Attractive photocatalyst approach in design parameters affecting the photocatalytic degradation. Catalysis Communications, 183 (August), 106764. 10.1016/j.catcom.2023.106764.
- [48] Chen, C., Zhao, C., Zhou, X., Chen, J., Chen, L., Li, F. (2021). DFT study on the interaction of H2O and O2 with α-Fe2O3 (001) surface. *Vacuum*, 188. 110-164. DOI: 10.1016/j.vacuum.2021.110164.
- [49] Li, J., Miao, X., Han, B., Wang, K., An, B., Xu, G., Ju, D., Li, Y., Yu, H., Zhou, W. (2024). Sulphonated coal tar pitch as a carbon source to develop the storage capacity of Fe2O3@C materials. Catalysis Today, 439(189), 114822. DOI: 10.1016/j.cattod.2024.114822.
- [50] Abu-Saied, M.A., Abualnaja, K.M., Eman A, El-Desouky Gamal, A.-N., E.A. Eldeeb, Elerian, A.F. (2024). Sulphonated poly (Glycidyl Methacrylate-co-Styrene)-based adsorbents for the removal of Methylene Blue (MB) dye from aqueous solutions. *Desalination and Water Treatment*, 320 (3), 23-33. DOI: 10.1016/j.dwt.2024.100759
- [51] Ramajeya, C., Balasubramanian, K. (2025). Lisoleucine doped Creatininium Benzene Sulphonate organic single crystals: Insight into charge carrier dynamics and sensor applications. Results in Engineering, 26(March), 104815. DOI: 10.1016/j.rineng.2025.104815.

- [54] Wang, Y., Fang, Z., Zhang, F. (2019). Esteri fi cation of oleic acid to biodiesel catalyzed by a highly acidic carbonaceous catalyst. *Catalysis Today*, 319(May 2018), 172–181. DOI: 10.1016/j.cattod.2018.06.041.
- [55] Wolski, L., Sobańska, K., Walkowiak, A., Akhmetova, K., Gryboś, J., Frankowski, M., Ziolek, M., Pietrzyk, P. (2021). Enhanced adsorption and degradation of methylene blue over mixed niobium-cerium oxide – unraveling the synergy between Nb and Ce in advanced oxidation processes. *Journal of Hazardous Materials*, 415(March), 125665. DOI: 10.1016/j.jhazmat.2021.125665.
- [56] Ulfa, M., Al Afif, H., Saraswati, T.E., Bahruji, H. (2022). Fast Removal of Methylene Blue via Adsorption-Photodegradation on TiO2/SBA-15 Synthesized by Slow Calcination. *Materials*, 15(5471), 1–13. DOI: 10.3390/ma15165471.

- [57] Kanakaraju, D., bin Ya, M.H., Lim, Y.C., Pace, A. (2020). Combined Adsorption/Photocatalytic dye removal by copper-titania-fly ash composite. Surfaces and Interfaces, 19(January), 100534. DOI: 10.1016/j.surfin.2020.100534.
- [58] Murphy, S., Saurel, C., Morrissey, A., Tobin, J., Oelgemöller, M., Nolan, K. (2012). Photocatalytic activity of a porphyrin/TiO2 composite in the degradation of pharmaceuticals. *Applied Catalysis B: Environmental*, 119–120, 156–165. DOI: 10.1016/j.apcatb.2012.02.027.